

# Supercriticality to subcriticality in dynamo transitions

Rakesh K. Yadav<sup>1,\*</sup> and Mahendra K. Verma<sup>1</sup>

<sup>1</sup>*Department of Physics, Indian Institute of Technology – Kanpur 208016, India*

## Abstract

In this paper, we present a three-mode dynamo model which describes both supercritical and subcritical dynamo transitions. The nature of dynamo transition changes from supercritical to subcritical as the magnetic Prandtl number is decreased, consistent with the numerical results in the spherical-shell and the Taylor-Green dynamo. We also perform a detailed analysis of the hysteresis zone of a subcritical dynamo using direct numerical simulations. Numerical simulation and model analysis show that the sets of initial conditions, called the basin of attraction, of the no-dynamo and the dynamo states are separated by an unstable manifold.

PACS numbers: 91.25.Cw, 47.20.Ky, 52.65.Kj

---

\*Email : yadav.r.k.87@gmail.com

## I. INTRODUCTION

Many natural and engineering systems exhibit transitions from one state to another. Some of the prominent examples of transitions are water to vapor, paramagnetic to ferromagnetic, conduction to convection (e.g, in Rayleigh Bénard convection), laminar to turbulent flow in channels, etc. Some of these transitions are continuous, i.e., the order parameter grows smoothly from zero as the control parameter is increased, while some others exhibit a discontinuity or a finite jump in the order parameter. The former class of transitions is called *supercritical*, while the latter is called *subcritical*.

Magnetic field generation or dynamo process in astrophysical systems exhibits transition from no-dynamo or fluid state to a magnetic state [1, 2]. This transformation is referred to as “dynamo transition”. Laboratory experiments report supercritical transition [3–6], but numerical simulation and models exhibit both supercritical [7–9] and subcritical transitions [9–14]. In this paper, we explain these transitions using a low-dimensional model and relate them to the strength of the nonlinear interactions.

Nature of dynamo transition can play a very crucial role in our understanding of astro and planetary dynamos. For instance, Mars is believed to have no working dynamo, but it exhibits strong crustal magnetism. Kuang *et al.* [15] conjectured that the sudden termination of the Martian dynamo could be due to a subcritical dynamo transition. Christensen *et al.* [7] and Morin and Dormy [16] used numerical simulations to study dynamo mechanism in rotating spherical-shells; they observed both supercritical and subcritical dynamo transitions in such systems. The control parameters for dynamo simulations are the magnetic Prandtl number  $Pm = \nu/\eta$ , the Reynolds number  $Re = UL/\nu$ , and the magnetic Reynolds number  $Rm = UL/\eta$ , where  $\nu, \eta$  are the kinematic viscosity and magnetic diffusivity respectively, and  $U, L$  are the large-scale velocity and length scales. These studies also indicate that the dynamo transition changes from supercritical to subcritical as the magnetic Prandtl number  $Pm$  is decreased. Similar dependence on  $Pm$  has been observed in the Taylor-Green dynamo [8, 10, 14] and shell models [12, 13]. Based on geometrical similarities and the aforementioned  $Pm$  dependence, Yadav *et al.* [14] conjectured a connection between the Taylor-Green dynamo and the spherical-shell dynamo.

Low-order dynamo models, despite of their simplicity, can nonetheless provide very interesting insights. Bullard [17] used a homopolar disk dynamo to study the basic dynamo

mechanism, and, subsequently, Rikitake [18] used a coupled disk dynamo model to qualitatively discern the geomagnetic reversals. Pétrélis and Fauve [19] constructed a low-order dynamo model based on amplitude equations involving dipolar and quadrupolar modes to study magnetic field reversals in the Von-Karman-Sodium (VKS) experiment [5, 20]. Later Gissinger *et al.* [21] proposed a three-mode model for similar analysis. Verma *et al.* [22] constructed a six-mode model to study the importance of helicity in dynamo transitions; they report a supercritical pitchfork dynamo transition. A subcritical dynamo transition has been demonstrated by Fedotov *et al.* [23] in a perturbative  $\alpha\Omega$ -dynamo model. Krstulovic *et al.* [9] devised a model containing two nonlinear equations to explain the Pm dependence of the supercritical and subcritical dynamo transition. Weiss [24] provides a detailed review of the low-order dynamo models which are related to the planetary and solar dynamos.

In this paper we construct a three-mode model that captures both supercritical and subcritical dynamo transition. The model shows a very good agreement with the recently performed numerical simulations of the Taylor-Green dynamo [8, 14].

The paper is structured in the following manner. In Sec. II, we discuss one-dimensional equations which show supercritical and subcritical bifurcations. Section III contains a simulation study of the Taylor-Green dynamo in a subcritical regime. We propose a three-mode model in Sec. IV. We conclude in Sec. V

## II. ONE-DIMENSIONAL MODEL

Our three-mode dynamo model, to be described later, is motivated by a one-dimensional (1D) model that exhibits supercritical and subcritical transitions [25, 26]. The first part of the model

$$\dot{X} = C_1 X + C_3 X^3, \tag{1}$$

exhibits supercritical transition. For negative values of  $C_3$ , the solution  $X = 0$  is stable for  $C_1 < 0$ . For  $C_1 > 0$ , this solution becomes unstable, and a new stable solution  $\sqrt{-C_1/C_3}$  is born. The bifurcation diagram for this system with  $C_3 = -1$  is illustrated in Fig. 1(a). Note that the new solution exists only when  $C_3 < 0$ ; for  $C_1, C_3 > 0$ , the above system is unstable.

When  $C_3 > 0$ , a higher-order term  $C_5 X^5$  with  $C_5 < 0$  is added to stabilize the system,

i.e.,

$$\dot{X} = C_1 X + C_3 X^3 + C_5 X^5. \quad (2)$$

Fig. 1(b) illustrates the bifurcation diagram of this system for  $C_3 = 1$  and  $C_5 = -1$ . It exhibits a subcritical pitchfork bifurcation and a jump in the value of  $X$  at the bifurcation point  $C_1 = 0$ . In addition, the system undergoes a saddle-node bifurcation at  $C_1 = -0.25$ . The hysteresis cycle represented by the arrows in Fig. 1(b) results due to these bifurcations. The hysteresis zone has multiple final states, as evident from Fig. 1(b). For  $-0.25 < C_1 < 0$ , initial conditions below the unstable manifold (solid curve connecting hollow red-dots) settle down to  $X = 0$  states (filled blue-dots on  $X = 0$  axis), while the ones above the unstable manifold settle down to  $X > 0$  states (filled blue-dots). A similar situation exists for the  $X < 0$  states. Thus, initial condition plays a critical role in determining the final state of a subcritical system. In the following discussion, we will construct a three-mode dynamo model that exhibits similar features as the aforementioned 1D model.

In the next section we report numerical results of a Taylor-Green dynamo in a subcritical regime. We show that the numerical results are in good agreement with the behavior of 1D model described by Eq. (2).

### III. SUBCRITICAL DYNAMO TRANSITION IN TAYLOR-GREEN DYNAMO

The fluid velocity  $\mathbf{u}$  and the magnetic field  $\mathbf{B}$  in dynamo mechanism are governed by the magnetohydrodynamic (MHD) equations:

$$\partial_t \mathbf{u} + (\mathbf{u} \cdot \nabla) \mathbf{u} = -\nabla p + (\mathbf{J} \times \mathbf{B}) + \nu \nabla^2 \mathbf{u} + \mathbf{F}, \quad (3)$$

$$\partial_t \mathbf{B} = \nabla \times (\mathbf{u} \times \mathbf{B}) + \eta \nabla^2 \mathbf{B}, \quad (4)$$

$$\nabla \cdot \mathbf{u} = 0, \quad (5)$$

$$\nabla \cdot \mathbf{B} = 0, \quad (6)$$

where  $\mathbf{J}$ ,  $\mathbf{F}$ ,  $p$ ,  $\nu$ , and  $\eta$  represent current density, external forcing, hydrodynamic pressure, kinematic viscosity, and magnetic diffusivity respectively. Note that  $\mathbf{J} = \nabla \times \mathbf{B}$ . The density

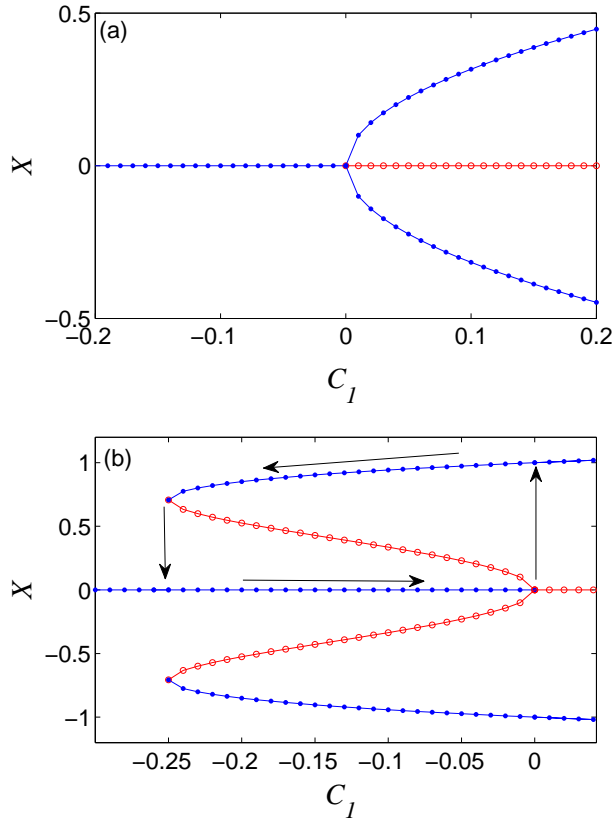


FIG. 1: (Color online) Bifurcation diagrams for Eq. (1) and Eq. (2) portraying (a) supercritical and (b) subcritical transitions. The filled-blue and the hollow-red dots represent the stable and unstable states. In figure (b), the arrows depict the hysteresis cycle of the subcritical transition.

of the fluid is chosen to be unity. The Taylor-Green (TG) forcing,

$$\mathbf{F}(k_0) = F_0 \begin{bmatrix} \sin(k_0 x) \cos(k_0 y) \cos(k_0 z) \\ -\cos(k_0 x) \sin(k_0 y) \cos(k_0 z) \\ 0 \end{bmatrix}, \quad (7)$$

is one of the popular forcing schemes to study dynamo transition [8–10, 14]. Here,  $F_0$  is the forcing amplitude, and  $k_0$  ( $=2$ ) defines the length scale of the forcing. Yadav *et al.* [8, 14] showed that dynamos with the TG forcing exhibit supercritical and subcritical dynamo transition for  $\text{Pm} = 1$  and  $\text{Pm} = 0.5$  respectively. It has been shown that dynamos with  $\text{Pm}$  lower than 0.5 could also be subcritical [10, 12]. Near the dynamo transition, the nature of the bifurcation reported by Yadav *et al.* [8, 14] is similar to the aforementioned 1D model.

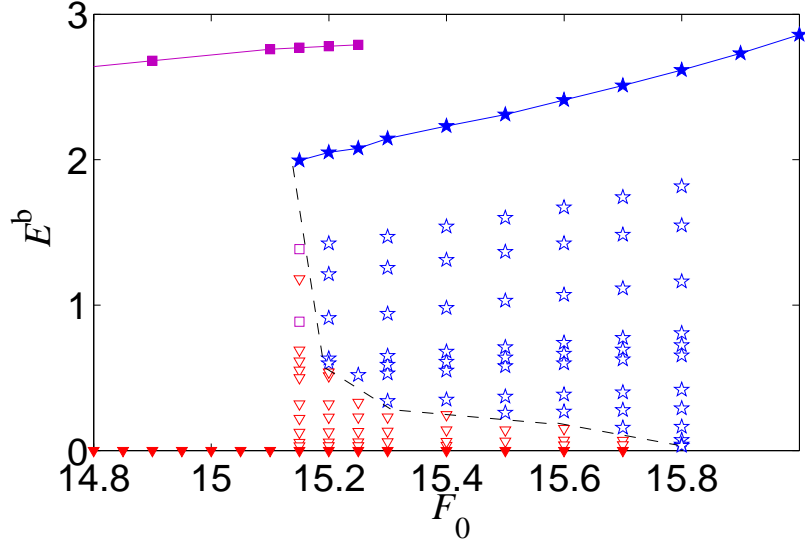


FIG. 2: (Color online) Bifurcation diagram constructed using various dynamo states of the TG dynamo. The filled blue-stars connected by solid line represent a stable dynamo branch. The runs with hollow blue-stars as initial conditions go back to the dynamo branch (filled blue-stars), while the runs with hollow red-triangles as initial conditions settle down to the no-dynamo states (filled red-triangles). The initial conditions denoted by hollow purple-squares near the hysteresis boundary stabilize to a different dynamo branch represented by filled purple-squares.

The reader is referred to the Fig. 4 of Ref. [8] (for  $\text{Pm} = 1$ ) and the Fig. 3 of Ref. [14] (for  $\text{Pm} = 0.5$ ), which are similar to Fig. 1.

Subcriticality in the dynamo transition has been inferred based on a jump in the magnetic energy and a hysteresis near the transition [10, 14, 27]. The generic subcritical bifurcation described by Eq. (2) exhibits more features, e.g., existence of subcritical-pitchfork and saddle-node bifurcations. Also, in the hysteresis window, the system stabilizes to either  $X = 0$  or  $X \neq 0$  depending on the initial condition. Using direct numerical simulations (DNS) we explore whether these rich features are present in the subcritical regime of the TG dynamo or not. We use a pseudospectral code Tarang [28] to numerically solve Eqs. (3)-(6) with  $\text{Pm} = 0.5$  ( $\nu = 0.1$  and  $\eta = 0.2$ ) in a cube of dimensions  $(2\pi)^3$  having periodic boundary conditions on all sides. We discretize the simulation box using  $64^3$  grid points. Interested reader is referred to Ref. [14] for more details about the numerical procedure.

Figure 2 contains results obtained using DNS of the TG dynamo for  $\text{Pm} = 0.5$ . As

reported by Yadav *et al.* [14], at  $F_0 = 15.8$  we first observe a fixed-point dynamo state (temporally non-fluctuating); here, the magnetic energy  $E^b$  shows a finite jump to  $\approx 2.6$  (the topmost star of the filled blue-star trail). However, when the dynamo state at  $F_0 = 15.8$  is used as an initial condition and the forcing amplitude is gradually decreased, the dynamo state continues along the trail till  $F_0 \approx 15.15$ , at which point there is a sudden dip to the fluid state (filled red-triangles). Thus,  $F_0 = 15.15 : 15.8$  is the hysteresis band for  $\text{Pm} = 0.5$  TG dynamo. To explore the basins of attraction of the  $E^b = 0$  and the  $E^b > 0$  states, we construct a set of initial conditions using the dynamo states on the filled blue-star trail.

For the initial conditions, we keep the velocity field same as that of the dynamo state, but the magnetic field is quenched by a factor, e.g., 2, 4, 6, etc. The set of initial conditions used in this work are indicated by hollow data points in Fig. 2. Interestingly, for a given  $F_0$ , all the runs with hollow blue-stars as initial conditions stabilize to the corresponding dynamo states (filled blue-stars). On the contrary, the runs with hollow red-triangles as initial conditions settle to the corresponding no-dynamo states (filled red-triangles). Thus, in the hysteresis zone, the regions with hollow blue-stars and hollow red-triangles form the basins of attraction of the dynamo and no-dynamo states respectively. The dashed black curve separates the two regions, a feature very similar to that observed for the subcritical system of Eq. (2).

Another feature appears in our simulation: the runs with the initial conditions denoted by hollow purple-squares stabilize to the corresponding filled purple-square dynamo state (at  $F_0 = 15.15$ ), which belongs to another dynamo branch. Note that this new branch originates from the edge of the hysteresis, and it is related to the high-dimensionality of the system. The other dynamo states on the purple trail were constructed using the filled purple-square dynamo state for  $F_0 = 15.15$ . The above analysis demonstrates that the system is very sensitive to the initial condition, and we need to keep this in mind while studying dynamo.

The TG dynamo under investigation has many degrees of freedom. Yet, similarities between the bifurcation diagrams of Fig. 1(b) and Fig. 2 indicate that the system dynamics could be understood using the important modes of the system. Yadav *et al.* [8, 14] showed that for the TG forcing with  $k_0 = 2$ , the most dominant velocity and magnetic Fourier modes are  $\mathbf{u}(2, 2, 2)$  and  $\mathbf{B}(0, 0, 1)$  respectively, and they couple via  $\mathbf{B}(-2, -2, -1)$  Fourier mode. The dominance of the large-scale modes is consistent with the results of the VKS experi-

ment [20] and the planetary dynamo simulations [7] in which the dipolar and quadrupolar magnetic field modes dominate near the transition. Motivated by these observations, we construct a three-mode model. We will show in the next section that this three-mode model captures the transition from supercritical to subcritical dynamo quite nicely.

#### IV. THREE-MODE DYNAMO MODEL

In our model, we consider a velocity mode  $u$  and two magnetic modes  $B_1$  and  $B_2$  which are coupled nonlinearly with each other. The equations of the model are

$$\dot{u} = f - \nu u - B_1 B_2, \quad (8)$$

$$\dot{B}_1 = \alpha u B_2 - \eta B_1, \quad (9)$$

$$\dot{B}_2 = u B_1 - \eta B_2 + \beta u B_1^3, \quad (10)$$

where  $\nu$  and  $\eta$  are the kinematic viscosity and magnetic diffusivity respectively,  $f$  is the external force acting on the velocity field, and  $\alpha, \beta$  are positive constants. The nature of the nonlinear interactions resembles the MHD interactions where  $\partial_t B(\mathbf{k}) \sim u(\mathbf{p})B(\mathbf{q})$  and  $\partial_t u(\mathbf{k}) \sim B(\mathbf{p})B(\mathbf{q})$  with  $\mathbf{k} = \mathbf{p} + \mathbf{q}$ . Also, our model respects the symmetry of the MHD equations under  $\mathbf{B} \rightarrow -\mathbf{B}$  transformation. The coefficients of the nonlinear terms  $uB_2$  and  $uB_1$  are different since  $B_1$  and  $B_2$  correspond to different wavenumbers. The cubic term  $uB_1^3$ , induced by a higher order of nonlinearity, plays an important role in dynamo transition of this model. Our model has certain similarities with that of Gissinger *et al.* [21] except the cubic interaction.

For the aforementioned model, the first dynamo state is a fixed point, which we study perturbatively. We compute fixed point solutions by setting the right-hand-side of Eqs. (8) and (10) to zero, which yields

$$B_2 = \frac{uB_1 + \beta uB_1^3}{\eta}, \quad (11)$$

$$u = \frac{f}{\nu} \left[ 1 + \frac{B_1^2(1 + \beta B_1^2)}{\nu\eta} \right]^{-1}. \quad (12)$$

Substitution of the above expressions of  $B_2$  and  $u$  in Eq. (9) provides

$$\dot{B}_1 = \frac{\alpha f^2}{\nu^2 \eta} (B_1 + \beta B_1^3) \left[ 1 + \frac{B_1^2(1 + \beta B_1^2)}{\nu\eta} \right]^{-2} - \eta B_1. \quad (13)$$



An approximation of Eq. (13) to the fifth order in  $B_1$  yields

$$\dot{B}_1 \approx \underbrace{\left[-\eta + \frac{\alpha f^2}{\nu^2 \eta}\right]}_{C_1} B_1 + \underbrace{\left[\frac{\alpha f^2}{\nu^3 \eta^2} (\nu \eta \beta - 2)\right]}_{C_3} B_1^3 + \underbrace{\left[\frac{\alpha f^2}{\nu^3 \eta^2} \left(\frac{3}{\nu \eta} - 4\beta\right)\right]}_{C_5} B_1^5. \quad (14)$$

Note that Eq. (14) has the same form as Eq. (2), and the nature of its transition is governed by the coefficients  $C_3$  and  $C_5$ .

The dissipative parameters  $\nu$  and  $\eta$  take positive values. In addition, we assume that  $\alpha, \beta > 0$ . Under these assumptions, the following properties can be deduced for  $C_1, C_3$ , and  $C_5$ :

1. For a given values of  $\nu$  and  $\eta$ ,  $C_1$  changes sign depending on the force parameter  $f$ , hence  $f$  is the control parameter.
2. The sign of  $C_3$  depends on the term  $(\nu \eta \beta - 2)$ . For a given  $\nu$ ,  $C_3 < 0$  for  $\eta < \eta_c = 2/(\beta \nu)$ , which provides a supercritical transition. For  $\eta > \eta_c$  or  $\nu \eta \beta > 2$ , we observe subcritical transition. We can deduce the critical magnetic Prandtl number  $\text{Pm}_c$  that separates the supercritical and subcritical dynamo using the condition  $\beta \nu \eta_c = 2$ , which yields

$$\text{Pm}_c = \frac{\nu}{\eta_c} = \frac{\beta \nu^2}{2}. \quad (15)$$

3. The sign of  $C_5$  is determined by  $(\frac{3}{4} - \nu \eta \beta)$ . For subcriticality, we require  $C_3 > 0$  and  $C_5 < 0$  (see Sec. II), which are satisfied by the condition  $\nu \eta \beta > 2$ .

Thus the structure of Eq. (14) is same as that of one-dimensional model discussed in Sec. II.

We construct a potential function for  $B_1$  using Eq. (14) as

$$\begin{aligned} V(B_1) &= - \int \dot{B}_1 dB_1 \\ &= -C_1 \frac{B_1^2}{2} - C_3 \frac{B_1^4}{4} - C_5 \frac{B_1^6}{6}. \end{aligned} \quad (16)$$

This function provides an elegant way of visualizing the nature of the dynamo states [25, 26]. In this description, the stable and the unstable dynamo states are represented by “valleys” and “hills”, respectively, of the potential function.

In the following discussion we will illustrate the supercritical and subcritical dynamo transitions exhibited by the three-mode model.

### A. Supercritical Transition

Here we present a representative example of a supercritical dynamo by taking  $\nu = 10$ ,  $\eta = 1.5$ ,  $\beta = 0.1$ ,  $\alpha = 2$  for which  $C_3 < 0$ . For these parameters,  $\text{Pm}_c = 5$  and  $\text{Pm} = 10/1.5 \approx 6.6$ . Here, dynamo transition takes place at

$$f_c = \frac{\nu\eta}{\sqrt{\alpha}} \approx 10.6. \quad (17)$$

Figure 3(a) presents the potential functions, which exhibit a valley at  $B_1 = 0$  for  $f < f_c$ , and two valleys at  $B_1 \neq 0$  (labeled by blue dots) for  $f > f_c$ . Hence, the no-dynamo states are stable for  $f < f_c$ , and the dynamo states are stable for  $f > f_c$ . A bifurcation diagram constructed using these states is illustrated in Fig. 3(b); filled-blue (hollow-red) dots are the stable (unstable) states.

### B. Subcritical Transition

To illustrate a subcritical dynamo transition in the three-mode model, we take  $\eta = 3$ , along with  $\nu = 10$ ,  $\beta = 0.1$ ,  $\alpha = 2$ . Here  $\text{Pm} = 10/3 \approx 3.3$ . These parameters yield  $C_3 > 0$  and  $C_5 < 0$ , thus yielding a subcritical dynamo transition. The critical forcing  $f_c$  for this set of parameters is  $30/\sqrt{2} \approx 21.2$ . Near  $f = f_c$ , we plot the potential functions and the bifurcation diagram in Fig. 4(a) and (b) respectively. At  $f = f_c$  we observe a finite jump in  $B_1$  (see Fig. 4(b)). As we decrease  $f$  from  $f_c$  with the above initial condition, the system continues to have nonzero  $B_1$  until  $f = f'_c \approx 20.94$ , after which it attains  $B_1 = 0$  state.

In the potential diagram of Fig. 4(a), we observe a single valley (stable state) at  $B_1 = 0$  for  $f \leq f'_c$ , and two valleys at  $\pm B_1$  and a hill at  $B_1 = 0$  for  $f \geq f_c$ . For  $f'_c \leq f \leq f_c$ , the system has three valleys and two hills. Depending on the initial condition, the system can “roll” to one of the valleys which explains the sensitivity to initial condition.

To better understand the role of initial condition on the final state of the system, we plot a separate potential function for  $f = 21.04$  in Fig. 5. This forcing value lies in between  $f'_c$  and  $f_c$ . If the initial condition lies on the dashed region of the potential function, then the system will roll down to the  $B_1 = 0$  valley (no-dynamo state). On the other hand, if the initial condition lies on the solid regions of the potential function, then the system will roll to either the  $B_1 > 0$  valley or the  $B_1 < 0$  valley, as indicated by the arrows; in these cases,

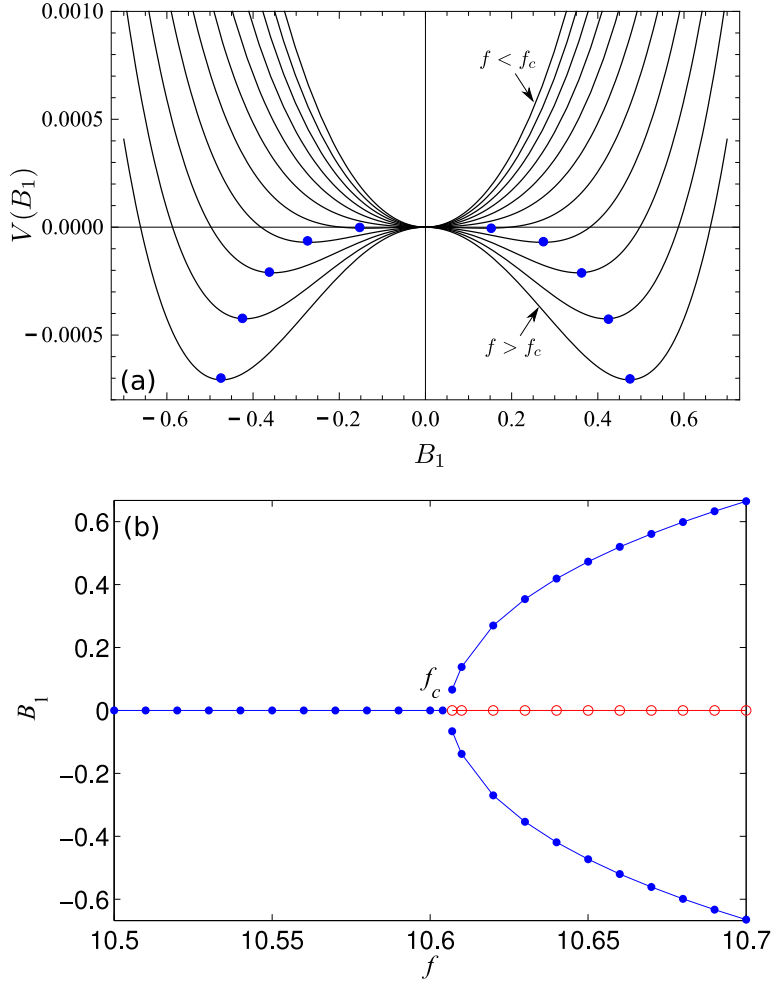


FIG. 3: (Color online) Plots of (a) Potential function, and (b) the corresponding supercritical transition of the dynamical system described by Eq. (14). We set  $\nu$ ,  $\eta$ ,  $\alpha$ , and  $\beta$  equal to 10, 1.5, 2, and 0.1 respectively. In the top panel, the forcing  $f$  is varied from 10.55 to 10.65 in steps of 0.01. Filled-blue (hollow-red) dots represent the dynamically stable (unstable) states.

the system will be a dynamo state. This behavior is applicable only for  $f'_c < f < f_c$ . For  $f > f_c$ , the two  $B_1 \neq 0$  unstable hills merge with  $B_1 = 0$  state.

The above results indicate that the three-mode dynamo model captures the supercritical to subcritical dynamo transition nicely. Moreover, this change in the nature of the dynamo transition is exhibited when we decrease the magnetic Prandtl number.

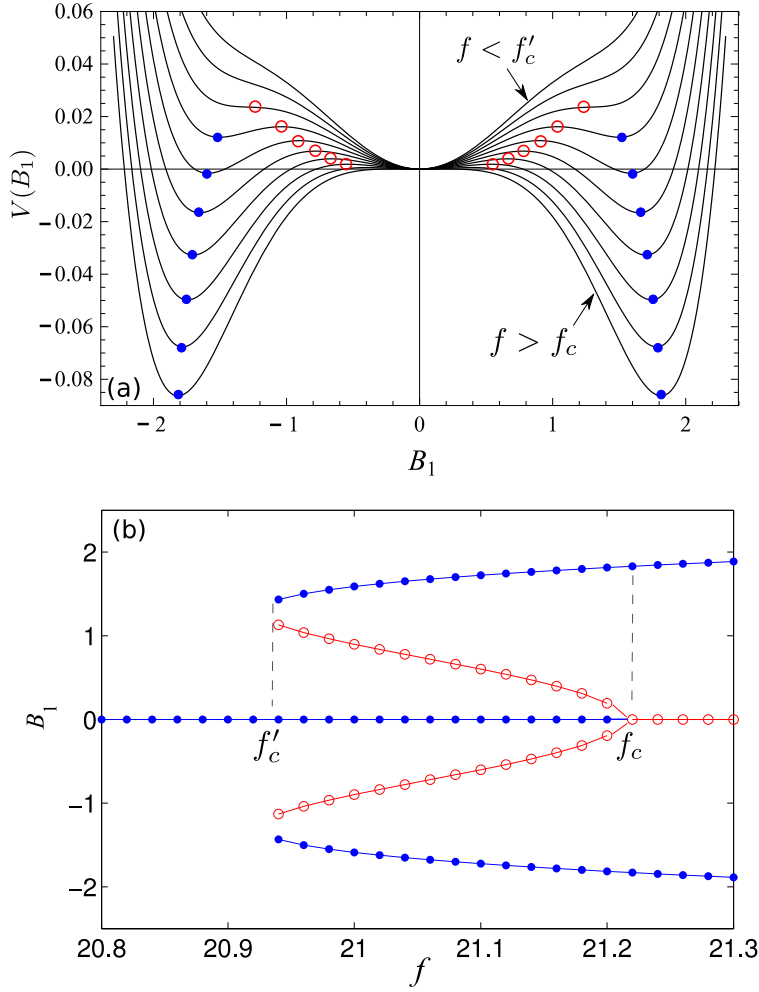


FIG. 4: (Color online) Plots of (a) Potential function, and (b) the corresponding subcritical transition described by Eq. (14). We set  $\nu$ ,  $\eta$ ,  $\alpha$ , and  $\beta$  equal to 10, 3, 2, and 0.1 respectively. In the top panel, the forcing  $f$  is varied from 20.84 to 21.2 in steps of 0.04. The filled-blue (hollow-red) dots represent the dynamically stable (unstable) states in both the figures.

## V. CONCLUSIONS AND DISCUSSIONS

In this paper, we construct a three-mode dynamo model motivated by the symmetries and the nature of the nonlinearities of the MHD equations. It contains a crucial third-order term  $B_1^3$ , a representative of a higher-order nonlinearity of the system. Our model exhibits both supercritical and subcritical dynamo transitions, with an interesting changeover from supercriticality to subcriticality as the magnetic Prandtl number is decreased. The above

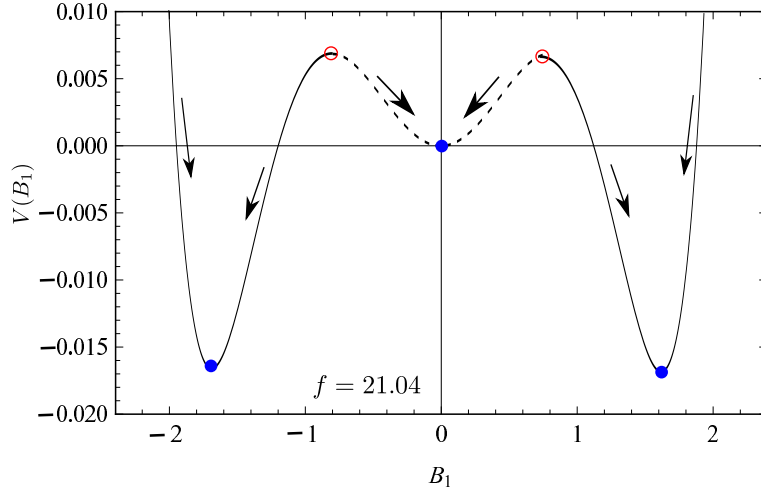


FIG. 5: (Color online) A plot of the potential function for  $f = 21.04$ . Here  $f'_c < f < f_c$ . The dashed curve represents the initial conditions for the no-dynamo state (filled blue-dot at  $B_1 = 0$ ), while the solid curve represents the initial conditions for the dynamo state (filled blue-dots at  $B_1 \neq 0$ ). The arrows represent the rolling direction of the dynamical system.

features are consistent with the numerical results of the Taylor-Green [8, 14] and spherical-shell dynamos [16]. VKS experiment, which exhibits supercritical dynamo for a very small Pm, appears to be contrary to the above behavior. The reason for this disagreement is not apparent at present; it could possibly be due to some stabilizing feature of cylindrical geometry employed in the experiment.

In our three-mode model, the dynamo transition depends crucially on the extent of stabilizing and destabilizing terms. Supercritical to subcritical transition takes place when the  $B_1^3$  term of Eq. (14) destabilizes the magnetic field, which is subsequently stabilized by an even higher order interaction  $B_1^5$  of the equation. This feature is similar to the recent findings of Sreenivasan and Jones [27] for subcritical spherical-shell dynamo in which the Lorentz force, which otherwise saturates the magnetic field, destabilizes it.

We also present a detailed analysis of the hysteresis region of a subcritical dynamo transition using direct numerical simulation and three-mode model. We show that the final state of a subcritical dynamo depends quite critically on the initial condition. The basin of attraction of the dynamo and the no-dynamo states are separated by a well-defined unstable manifold.

The potential function described in this paper has some similarities with those observed in the Maxwell's construction in equilibrium thermodynamics as well as phenomenon like supercooling. It may be interesting if some features like initial condition sensitivity and multiple states discussed in our paper could be observed in such systems for some exceptional cases.

In summary, our dynamo model exhibits supercritical and subcritical dynamo transitions. The model also shows a changeover from supercriticality to subcriticality when the magnetic Prandtl number is decreased. It would be interesting to make quantitative comparisons of the model with realistic dynamos. However, the analysis of the large number of modes in such systems is very complex, which may be possible in future studies.

## VI. ACKNOWLEDGMENTS

We thank K. P. Rajeev, H. Wanare, and T. Sarkar for useful suggestions and discussions. The numerical simulations were performed on CHAOS cluster (IIT Kanpur) and the VEGA cluster (IIT Madras). The authors also acknowledge the research grant SPO/BRN-S/PHY/20090310 and the Swarnajayanti fellowship to M. K. Verma.

- 
- [1] H. K. Moffatt, *Magnetic Field Generation in Electrically Conducting Fluids* (Cambridge university press, Cambridge, 1978).
  - [2] A. Brandenburg and K. Subramanian, Phys. Rep. **417**, 1 (2005).
  - [3] A. Gailitis, O. Lielausis, E. Platacis, S. Dement'ev, A. Ciferons, G. Gerbeth, T. Gundrum, F. Stefani, M. Christen, and G. Will, Phys. Rev. Lett. **86**, 3024 (2001).
  - [4] R. Stieglitz and U. Müller, Phys. Fluids **13**, 561 (2001).
  - [5] R. Monchaux, M. Berhanu, M. Bourgoin, M. Moulin, P. Odier, J. Pinton., R. Volk, S. Fauve, N. Mordant, F. Pétrélis, et al., Phys. Rev. Lett. **98**, 044502 (2007).
  - [6] F. Pétrélis, N. Mordant, and S. Fauve, Geophys. Astrophys. Fluid Dyn. **101**, 289 (2007).
  - [7] U. Christensen, P. Olson, and G. A. Glatzmaier, Geophys. J. Intl. **138**, 393 (1999).
  - [8] R. Yadav, M. Chandra, M. K. Verma, S. Paul, and P. Wahi, Europhys. Lett. **91**, 69001 (2010).

- [9] G. Krstulovic, G. Thorner, J.-P. Vest, S. Fauve, and M. Brachet, Phys. Rev. E **84**, 066318 (2011).
- [10] Y. Ponty, J. Laval, B. Dubrulle, F. Daviaud, and J. Pinton, Phys. Rev. Lett. **99**, 224501 (2007).
- [11] F. Rincon, G. Ogilvie, M. Proctor, and C. Cossu, Astronomische Nachrichten **329**, 750 (2008).
- [12] G. Sahoo, D. Mitra, and R. Pandit, Phys. Rev. E **81**, 036317 (2010).
- [13] G. Nigro and P. Veltri, ApJ Lett. **740**, L37 (2011).
- [14] R. K. Yadav, M. K. Verma, and P. Wahi, Phys. Rev. E **85**, 036301 (2012).
- [15] W. Kuang, W. Jiang, and T. Wang, Geophys. Res. Lett. **35**, L14204 (2008).
- [16] V. Morin and E. Dormy, Int. J. Mod. Phys. B **23**, 5467 (2009).
- [17] E. Bullard, Proc. Cambridge Philos. Soc. **51**, 744 (1955).
- [18] T. Rikitake, Proc. Cambridge Philos. Soc. **54**, 89 (1958).
- [19] F. Pétrélis and S. Fauve, Journal of Physics: Condensed Matter **20**, 494203 (2008).
- [20] F. Ravelet, M. Berhanu, R. Monchaux, S. Aumaître, A. Chiffaudel, F. Daviaud, B. Dubrulle, M. Bourgoïn, P. Odier, N. Plihon, et al., Phys. Rev. Lett. **101**, 074502 (2008).
- [21] C. Gissinger, E. Dormy, and S. Fauve, Europhys. Lett. **90**, 49001 (2010).
- [22] M. K. Verma, T. Lessinnes, D. Carati, I. Sarris, K. Kumar, and M. Singh, Phys. Rev. E **78**, 036409 (2008).
- [23] S. Fedotov, I. Bashkirtseva, and L. Ryashko, Phys. Rev. E **73**, 066307 (2006).
- [24] N. O. Weiss, Geophys. Astrophys. Fluid Dyn. **105**, 256 (2010).
- [25] S. H. Strogatz, *Nonlinear Dynamics And Chaos: With Applications To Physics, Biology, Chemistry, And Engineering (Studies in Nonlinearity)* (Westview Press, Cambridge, Massachusetts, 2001).
- [26] J. K. Bhattacharjee, S. Chakraborty, and A. K. Mallik, *Nonlinear Dynamics Primer with Applications to Magnetohydrodynamics* (Prism Books, 2011).
- [27] B. Sreenivasan and C. A. Jones, J. Fluid Mech. **688**, 5 (2011).
- [28] M. K. Verma, A. Chatterjee, S. Paul, S. Reddy, R. K. Yadav, M. Chandra, and R. Samtaney, arXiv:1203.5301v1 (2012).